



CHALMERS
UNIVERSITY OF TECHNOLOGY

Piezoelectric energy harvesting using stochastic resonance in rotating systems

Master's thesis in Nanotechnology

GUSTAV FORSBERG

MASTER'S THESIS

**Piezoelectric energy harvesting using
stochastic resonance in rotating systems**

GUSTAV FORSBERG



CHALMERS
UNIVERSITY OF TECHNOLOGY

Department of Microtechnology and Nanoscience
CHALMERS UNIVERSITY OF TECHNOLOGY
Gothenburg, Sweden 2019

Piezoelectric energy harvesting using stochastic resonance in rotating systems
GUSTAV FORSBERG

© GUSTAV FORSBERG, 2019.

Supervisor: Cristina Rusu, RISE AB

Examiner: Per Lundgren, Microtechnology and Nanoscience, Elektronikmaterial och system

Master's Thesis

Department of Microtechnology and Nanoscience

Chalmers University of Technology

SE-412 96 Gothenburg

Telephone +46 31 772 1000

Typeset in L^AT_EX

Printed by [Name of printing company]

Gothenburg, Sweden 2019

GUSTAV FORSBERG

Department of Microtechnology and Nanoscience
Chalmers University of Technology

Abstract

Sensors can be found virtually anywhere in today's society. With the ever developing technologies around us, the number of sensors is set to increase even faster in the near future. The Internet of Things and self-driving cars are just some of the emerging technologies that use huge amounts of sensors, and with these sensors comes the power demand of each of them. Today batteries are still the dominant power supply for sensors, however, energy harvesting technologies are in development to replace them.

This thesis examines the possibility to use a piezoelectric harvester to power a sensor mounted on a flexplate in a combustion engine. By studying current technologies, a concept was established and with simulations and experiments it was evaluated. The concept combined two previous designs and eliminated components previously used, creating a smaller harvester. The final harvester was based on an off the shelf piezoelectric harvester where the proof mass and placement of the harvester was simulated in order to optimize the performance. The simulation on the final design show a peak power of 370 μW and a 3 dB bandwidth of 2.44 Hz, promising results that could be used as the foundation in the development of a functional harvester.

Keywords: Piezoelectric, energy harvesting, stochastic resonance, rotation, cantilever, vibration.

Acknowledgements

There have been many challenges during this thesis and I have learned a ton, especially in concept generation as it was totally new to me. Now that the thesis is done, I have multiple people that needs to be mentioned as they have helped me significantly along the way.

I want to give a huge thank you to my examiner, Per Lundgren at Chalmers, for all the help and guidance during the thesis as well as all the input on my report. I also want to thank my supervisor, Cristina Rusu at RISE, for the opportunity of doing this thesis and the help along the way. I also want to thank Agin Vyas for all the help with COMSOL and Gabor Gereb for all the time and help during the experiments.

Thank you all for making this thesis possible!

Gustav Forsberg, Gothenburg, June 2019

Contents

List of Figures	x
I Introduction	1
1 Aim	2
1.1 Specifications	2
2 Energy harvesters	2
2.1 Strain harvesters	3
2.2 Vibrational energy harvesters	3
2.3 Rotational energy harvesters	4
2.3.1 Concept to evaluate	5
II Theoretical Background	7
3 Stochastic resonance	7
3.1 Stochastic resonance in energy harvesting	8
4 Piezoelectric power generation	11
4.1 The Piezoelectric effect	11
4.2 Piezoelectric materials	12
4.3 Power circuit	13
III Modelling and simulation	15
5 Design	16
5.1 Redefining variables	16
5.2 Harvester parameters	17
6 Solving the equation of motion in MATLAB	18
7 Numerical simulations in COMSOL	18
7.1 Geometry	19
7.2 Materials	19
7.3 Boundary conditions	19
7.3.1 Solid Mechanics	20
7.3.2 Electrostatics	20
7.4 Mesh	20
7.5 Study steps	21
7.6 Visualization of results	21

IV	Experiments	22
8	Method	22
8.1	Frequency and resistance sweeps	23
8.2	Damping	24
8.3	Buckling	25
V	Results and Discussion	26
9	Results	26
9.1	Experimental and COMSOL	27
9.2	Equation of motion simulation	29
10	Discussion	32
10.1	Future work	33
VI	Conclusion	34
	References	35

List of Figures

2.1	Different designs of two-degree-of-freedom micro-cantilevers by Vyas et al. [10]. Figure provided by Vyas and printed with permission.	4
2.2	Sketch of the concept and the movement between the stable positions created by the centrifugal force. The different aspects of the concept are explained in part II.	6
3.1	Magnetically induced bistable system with A) only interwell movement, B) movement between stable positions.	9
4.1	Design of a basic piezoelectric cantilever.	12
4.2	Bimorph piezoelectric beams configured in A) parallel and B) series.	12
4.3	Crystal structure of PZT [28].	13
4.4	Basic power circuit for piezoelectric harvesters.	14
7.1	Harvester model in COMSOL.	19
7.2	The mesh outline of the model in COMSOL, PZT-5J shown in blue.	20
8.1	Experimental setup for frequency and resistance sweeps.	23
8.2	Experimental setup for the static buckling experiment with the harvester mounted on an adjustable setup in order to apply force.	24
8.3	Experimental setup for rotation testing in the horizontal configuration.	25
9.1	The resistance sweeps in COMSOL and experimental showing the power at resonance dependent on resistance of a harvester without proof mass.	27
9.2	Displacement over time of the harvester with the peak positions marked for use in damping calculations.	27
9.3	The equilibrium positions of the double potential as a function of rotation frequency. The critical buckling frequency is seen at 3 Hz, where the system becomes bistable.	28
9.4	Theoretic bending of the harvester with experimental bending added as blue circles, the experimental buckling frequency as red and the calculated lower limit of buckling frequency as green.	28
9.5	Simulation of the displacement over time of the tip of the harvester under the cases: only alternating gravity and alternating gravity and added white noise.	29
9.6	The velocity as a function of displacement for the proof mass when only excited by alternating gravity.	30
9.7	The velocity as a function of displacement for the proof mass when SR occurs under excitation by alternating gravity and white noise.	30
9.8	The power output as a function of rotation frequency showing a peak power of 370 μ W and a bandwidth at 3 dB of 2.44 Hz.	31

- 9.9 Bandwidth comparison between the concept harvester and a harvester with the same Q-factor as obtained from the measured damping ratio. 31

Part I

Introduction

Sensors can be found virtually anywhere in today's society, from gyroscopes in our phones to pollution sensors in large factories. With the continued development of smartphones, smart homes, Internet of Things and the emergence of autonomous cars, the number of sensors around us will continue to increase and according to one market research report it is expected to be a \$241 billion market by 2022 [1].

A big player in the sensor market is the automotive industry. Modern cars have between 60-100 sensors each, a number that is predicted to increase [2]. For autonomous cars this number will most likely rise even higher, making sensors and adjacent technologies very interesting for the automotive industry of today.

As the technology is developing and new applications for sensors are found, new challenges also emerge. Some of the measurements that could be of great value require sensors to be placed in rough or remote environments where it is difficult to supply the sensors with energy. In these cases, batteries are the main source of energy for independent sensors. Two of the big problems with batteries are that they need to be replaced frequently, increasing maintenance costs, and the spent batteries need to be disposed in an environmentally friendly way, problems that will get even worse with an increasing number of sensors.

Different techniques for harvesting energy from the ambient environments have been developed and make use of energy such as solar and vibration energy. These techniques have shown great potential in replacing batteries for sensors, allowing the sensors to be powered by the ambient energy eliminating the need of replacement as the ambient energy does not run out.

This thesis is part of the second phase of the Vinnova project under the title "Miniaturized self-powered industrial sensor systems using energy harvesting technologies - Energy Supply Toolkit". In the first phase of the project different possible applications for energy harvesters were identified and the goal of the second phase of the project is to generate multiple concepts for evaluation before the third and final phase. The specific application in focus for this thesis is for the automotive industry, more specifically for a sensor mounted on the flexplate of an engine. The flexplate is the part that connects the crank shaft to the automatic transmission to transfer power.

This thesis is divided into six parts. The first part is the introduction where the aim of the project, the given specifications as well as currently available concepts are presented. From these ideas and designs the concept for this thesis is generated and in the second part of the thesis, theoretical background, the techniques that are used are explained more in depth. For the third part the design of the harvester is presented together with the numerical simulations that will be used to evaluate the concept. In the fourth part, a number of experiments are defined to give some experimental validation. Part five shows the result of the simulations, measurements

from the experiments with discussion, and finally, part six presents the conclusion of the thesis.

1. Aim

One of the possible applications that was identified in the first phase of the Vinnova project was a harvester for a strain sensor mounted on the flexplate of an engine. The aim of this thesis is to identify and evaluate a feasible harvesting concept that could replace the currently used battery for the sensor, making it possible to create an embedded self-powered system. The concept will be based on piezoelectric energy harvesting for a rotating system with large vibrations. A large part of the work focuses on earlier concepts for similar applications and the adaptation to the design specifications that is presented in section 1.1.

1.1 Specifications

The goal specifications of the harvester are that the dimensions of the harvester should be within 40x8x6 mm, where the most important is that it does not extend further than 6 mm out from the plane of the flexplate. The entire harvester should be mountable on the flexplate and it should be able to function in temperatures ranging from -40 to 150 °C and weigh no more than 50 g.

2. Energy harvesters

The main sources of ambient energy that were identified early in the project can be divided into three groups: strain, vibration and rotation. In this section examples of harvesters utilizing these energy sources will be shown and discussed. The examples shown are chosen from a large sample of harvesters as they represent some of the better performing alternatives in literature. Some examples will also be shown in order to illustrate how they deal with limitations that similar techniques are affected by.

2.1 Strain harvesters

Strain energy harvesters couple directly to the deformation of the substrate or mechanical source to which it is attached [3]. These deformations can be things like the compression of the roadway when vehicles pass. Guiliano et al. reported an output power of 12.16 mW using a flexible piezoelectric macro-fiber composite with an active area of 85x28 mm² under 1170 $\mu\epsilon$, where $\epsilon = \frac{\Delta L}{L}$ and L is the length and ΔL is the elongation under strain., and a frequency of elongation of 10Hz. This was achieved by applying an alternating longitudinal force of 24 kN to the aluminium substrate that the harvester was attached to [4].

Arms et al. reported a piezoelectric harvester that was attached to the pitch link on a Bell 412 helicopter with an output of up to 400 μW for $\pm 35 \mu\epsilon$ at 15 Hz with a similar design [5].

To use strain harvesters such as the ones by Guiliano et al. and Arms et al. the strain needs to be alternating. However, in our case, the strain in a flexplate mainly changes during acceleration and deceleration. For constant rotation speeds the change in strain is mostly small, thus making the available energy small. So even if the strain changes during acceleration could be enough to supply the sensor it would only work a very short period until the desired speed is reached. This makes the strain of the flexplate less likely to be suitable as the main source of energy for an energy harvester. Strain energy harvesters have the advantage that they do not extend far out from the surface to which they are attached.

2.2 Vibrational energy harvesters

Vibrational energy harvesters are widely discussed in literature and piezoelectric harvesters are often used for small applications. Piezoelectric harvesters is further described in section 4.1. Multiple review articles on piezoelectric energy harvesting are available and a comprehensive comparison between different harvesting techniques are presented in a review paper written by Narita et al. [6]. The authors compared harvesters made between 2015-2017 and found that for piezoelectric harvesters, excluding microelectromechanical systems (MEMS) based harvesters, the range is 1.62-1600 mm³ in size and 18-5800 μW in power output. A review by Kim et al. addresses vibration based piezoelectric harvesting more specifically and contains both the main principles such as cantilever type, stack type, etc. and specific harvester designs from multiple sources [7].

One major problem for vibration based harvesters, especially piezoelectric, is that they often have very narrow bandwidth. This means that the harvester only gives high output for a very limited range of frequencies. Broadening the bandwidth of harvesters is a task that numerous researchers are working on with many different concepts. Xu et al. uses a pendulum attached to a cantilever obtaining energy harvesting from excitations from 3-dimensions as well as a broader bandwidth compared to a single cantilever [8]. Zhang et al. designed a multibeam matrix with springs connecting the beams and reported large improvements in bandwidth by adjusting the end masses of the different beams [9]. Vyas et al. demonstrated and analyzed

two-degree-of-freedom designs of micro-cantilevers, shown in figure 2.1, reporting harvesting capabilities in a range from 1293 Hz to 1781 Hz [10].

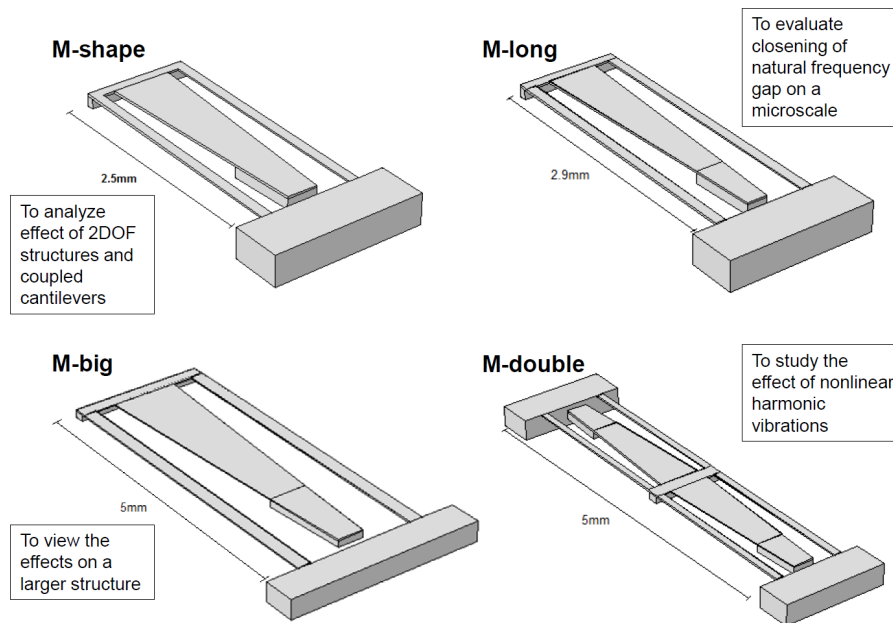


Figure 2.1: Different designs of two-degree-of-freedom micro-cantilevers by Vyas et al. [10]. Figure provided by Vyas and printed with permission.

For vibrations of the flexplate that are in a range of 10-1000 Hz, it is very hard to get a reliable output as it is too wide spectrum. Based on the wide spectrum of the vibration of the flexplate it should not be the main source of energy.

2.3 Rotational energy harvesters

The rotational aspect of the flexplate is the characteristic that shows greatest potential in supplying the energy to be harvested. This is because in rotating systems there are multiple sources of excitation that can be harvested, such as alternating gravity, centrifugal force and the rotational movement itself, all well defined by the rotation speed. When it comes to rotation based energy harvesters there are a broad variety of designs in the literature.

Multiple designs are based on having at least 2 separate parts, where one is static, and one is rotating. One of the better performing concepts based on this is by Wang et al. who reported a harvester using magnetostatic coupling between a static magnet array and rotating magnetic solenoids attached on a wheel. The authors reported a prototype for speeds of 10-60 mph (16-97 km/h) that had an output density of 1-5 W/cm³ [11]. However, as one of the specifications was that the harvester should be able to be mounted on the flexplate, designs with static parts are disregarded.

Devices mounted entirely on the rotating part of a system have a multitude of designs using the alternating gravity of the rotation as a source of excitation. Ming Li et al. combined a cantilever beam with a magnetostrictive/piezoelectric transducer,

using the alternating gravity of a rotating system to harvest energy. The author reported an output of $157.4 \mu\text{W}$ at a rotation rate of 588 rpm [12]. Using only piezoelectric harvesting Guan et al. reported an output of $83.5\text{-}825 \mu\text{W}$ for rotation frequencies of 7-13.5 Hz. The design had a cantilever with the tip mass at the centre of rotation to minimize the centrifugal force on the harvester [13]. Gu et al. took a different approach and made a passively tuned, outward oriented, piezoelectric energy harvester that used the centrifugal force to tune the resonance frequency. The authors reported a maximum output of 0.7 mW and a tenfold increase in bandwidth when compared to a cantilever with constant axial force [14].

For some rotating systems there is also vibration present within the system. A simple example is the vibration in a car's wheels that originate from the roughness of the road when driving. The range 10-10000 Hz for vibrations can be seen in the wheels of a car as concluded by Löhndorf et al. in a paper on energy harvesting concepts [15]. These conditions have been exploited in different concepts using stochastic resonance, that will be discussed more in detail in section 3.1. A summary of the use of stochastic resonance in this application is that it allows for movement between the two stable positions in a bistable system.

Zhang et al. used an outward oriented piezoelectric cantilever with a magnet as tip mass combined with a frame containing another magnet to create a bistable system. The authors reported movement between the stable positions both numerically and experimentally and reported an output ten times higher than a monostable system under the same excitation [16].

Kim et al. later used the centrifugal force on an inward oriented beam to generate the bistable system, thus allowing the system to be tuned based on the rotation speed. The harvester proposed by the author used an electromagnetic transducer with magnets and coils to get a high power output. The author reported not only a peak power of 45 mW but also movement between the stable systems for multiple frequencies up to an off-tuning frequency, increasing the bandwidth significantly compared to non self-tuning concepts [17, 18].

2.3.1 Concept to evaluate

Considering all the papers mentioned so far, the aim is to combine mainly the designs from Zhang et al. [16] and Kim et al. [17, 18] as these designs show great potential in power output and possibility to work for the specific application of this project. The concept will be based on a piezoelectric beam with a proof mass that is inwards oriented to create a bistable system using centrifugal force. This design allows the harvester to be much smaller than previous designs as it does not need any magnets to create the bistable system nor does it need coils for power generation. The smaller size could allow for the harvester and sensor to be embedded into one unit in a final design. A basic sketch of the concept is shown in figure 2.2.

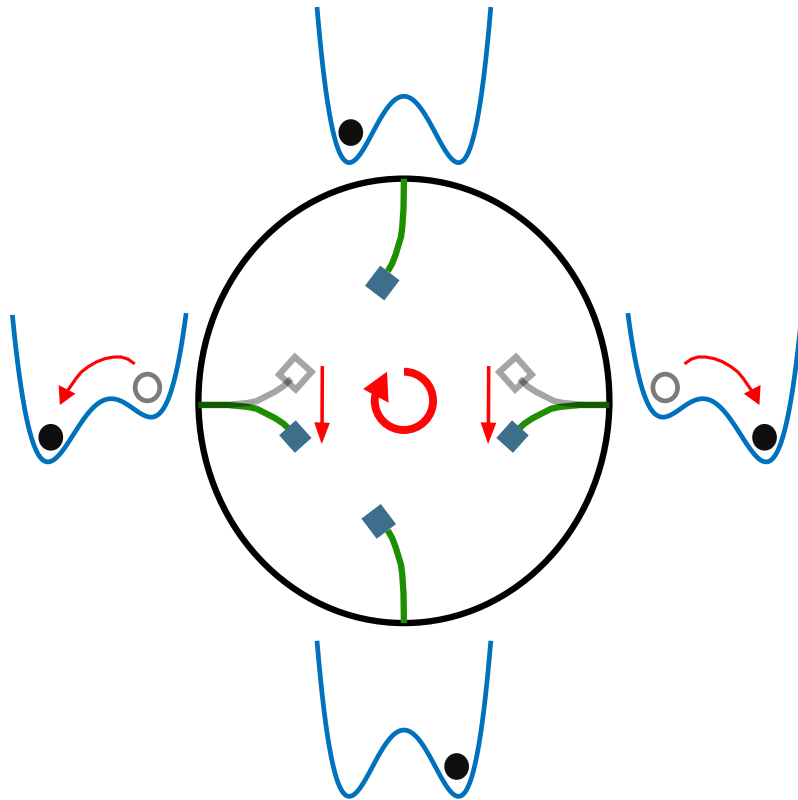


Figure 2.2: Sketch of the concept and the movement between the stable positions created by the centrifugal force. The different aspects of the concept are explained in part II.

Part II

Theoretical Background

The foundation of the proposed harvester concept that will be evaluated is presented in this section, starting with a brief introduction on what stochastic resonance is and then showing how it can be used to improve harvester possibilities. Further, the concept of piezoelectric energy harvesting will be described showing how the mechanical energy can be converted to electrical energy.

3. Stochastic resonance

The term stochastic resonance (SR) was coined in 1981 by Benzi et al. [19]. The author proposed that dynamical systems could show a resonance that was present when it was subjected to both noise and a periodic forcing but not when either of the parts was absent. From the coining of the term the phenomenon of SR has been found or used in many different fields, from optical systems, such as bistable ring lasers, to chemical reactions and neurophysiological processes [20]. The fact that an increase of noise input in the system can lead to an improvement of the signal-to-noise ratio of the output makes SR very interesting [21].

3.1 Stochastic resonance in energy harvesting

Stochastic resonance has been used in many fields as a tool for signal amplification by noise and have also found its way to energy harvesting. In 2008, McInnes et al. reported an increase in available power when a periodic forcing was added to a vibrationally excited energy harvester making use of SR [22].

SR constitutes the foundation of the energy harvester concepts presented by Zhang et al. [16] and Kim et al. [17, 18]. Energy harvesters that uses SR have three conditions that need to be fulfilled simultaneously. Firstly, the system needs to be bistable, thus have a double well potential, secondly, there needs to be a weak periodic signal, and thirdly, there needs to be an inherent noise (white noise). For the concept by Zhang et al. the author uses a magnet to get the bistable system allowing the equation of motion to be written as

$$m\ddot{x} + c\dot{x} - k_1x + k_3x^3 = N(t) + \epsilon \sin(\Omega t) \quad (3.1)$$

where x is the tip displacement of the beam, m is the proof mass at the tip, c is the damping coefficient, $-k_1 = a - M_{lin}$ and $k_3 = b - M_{nonlin}$, where a and b correspond to the linear and cubic stiffness of the beam respectively, modified by the linear and nonlinear magnetic coefficients M_{lin} and M_{nonlin} . $N(t)$ is the noise excitation and $\epsilon \sin \Omega t$ is the weak periodic signal with a small amplitude of ϵ and the frequency Ω . The t is for time and the overhead dots represents time derivatives.

The power that can be harvested can be derived by splitting the damping coefficient into mechanical damping, c_m , and electrically induced damping, c_e , and multiplying both sides of equation 3.1 with \dot{x} which gives

$$m\dot{x}\ddot{x} + (c_m + c_e)\dot{x}^2 - k_1x\dot{x} + k_3x^3\dot{x} = N(t)\dot{x} + \epsilon \sin(\Omega t)\dot{x} \quad (3.2)$$

and can be rearranged into

$$\frac{d}{dt} \left(\frac{1}{2}m\dot{x}^2 - \frac{1}{2}k_1x^2 + \frac{1}{4}k_3x^4 \right) + (c_m + c_e)\dot{x}^2 = N(t)\dot{x} + \epsilon \sin(\Omega t)\dot{x}. \quad (3.3)$$

Equation 3.3 shows that the instantaneous power into the system is equal to the rate of change of the sum of potential and kinetic energy plus the instantaneous power absorbed by the damping. In the parenthesis on the left side in equation 3.3 the systems kinetic energy is given by $\frac{1}{2}m\dot{x}^2$ and the potential energy by $-\frac{1}{2}k_1x^2 + \frac{1}{4}k_3x^4$. As $(c_m + c_e)\dot{x}^2$ represents the instantaneous power dissipated by damping, $c_e\dot{x}^2$ corresponds to the power that can be converted to electricity. Thus, the instantaneous power that can be harvested is given by

$$P = c_e\dot{x}^2. \quad (3.4)$$

The potential for the system where no periodic signal is applied can be written as

$$U(x) = -\frac{1}{2}k_1x^2 + \frac{1}{4}k_3x^4 \quad (3.5)$$

and when the periodic signal is added it becomes

$$U(x) = -\frac{1}{2}k_1x^2 + \frac{1}{4}k_3x^4 - \epsilon x \sin(\Omega t). \quad (3.6)$$

When the only excitation of the beam is done by the noise the movement will primarily be within one potential well, and movement between the wells can be estimated using the Kramers rate [23]

$$r_{kr} = \frac{k_1\sqrt{2}}{2\pi} \exp\left(-\frac{\Delta U}{D}\right) \quad (3.7)$$

where $\Delta U = \frac{-k_1}{4k_3}$ is the height of the potential barrier, D is the intensity of the noise given by $N(t) = \sqrt{2D}\xi(t)$ where $\xi(t)$ is Gaussian white noise. For $\Delta U \gg D$ the rate of movement between potentials becomes very small. By adding the weak periodic signal to the system, the potential is tilted, as can be seen in figure 3.1, increasing the probability of movement between the potential wells. When the weak periodic excitation synchronizes with the noise induced hopping, SR will occur, and the movement will be between the two potential wells at the rate of the weak periodic excitation. For this to happen the frequency of the periodic signal needs to match with half the Kramers rate giving the SR frequency as

$$f_{SR} = \frac{r_{kr}}{2} = \frac{k_1\sqrt{2}}{4\pi} \exp\left(-\frac{\Delta U}{D}\right). \quad (3.8)$$

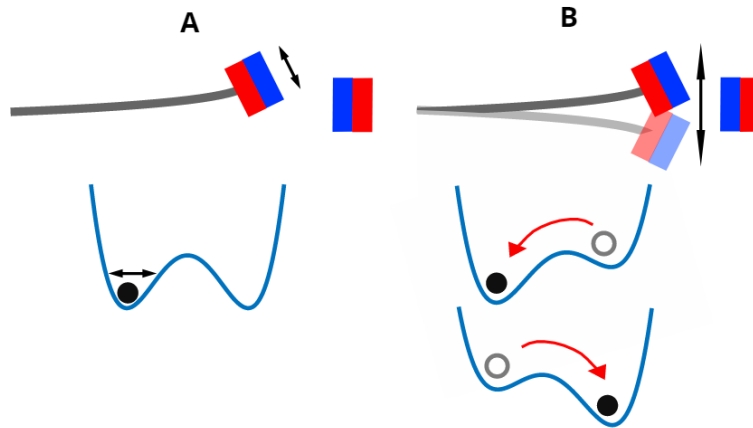


Figure 3.1: Magnetically induced bistable system with A) only interwell movement, B) movement between stable positions.

With the design used by Zhang et al., where permanent magnets are used to generate the bistable potential, the terms k_1 and k_3 are fixed and thus the SR only occurs in a narrow range of frequencies [16]. This design can be seen in a simplified version in figure 3.1.

By using a different method to generate the bistable system Kim et al. tries to overcome this limiting factor [17, 18]. The authors' design uses an inwards oriented beam and the centrifugal force to create bending in the beam and thus a bistable system. The authors also note that the noise intensity D increases linearly with the

rotation speed. In their paper the equation of motion is derived using the method of Turhan et al. [24]. The equation is approximated by the first vibration mode and given as

$$q'' + 2\zeta\lambda^4 q' + k_1 q + k_3 q^3 = K\epsilon n(\tau) \sin(\beta\tau) + K\epsilon \sin(\beta\tau) \quad (3.9)$$

where q is the generalized coordinate of the first mode, ζ is the damping ratio defined as the damping coefficient, c , divided by the critical damping coefficient, c_c , λ is the eigenvalue of the first mode, $\beta = \Omega/\omega_0$ is the dimensionless rotation speed normalized by $\omega_0 = \sqrt{\frac{EI}{\rho w t L^4}}$, where E and I is the Young's modulus and the moment of inertia of the beam respectively, w, t and L is the width, thickness and length of the beam. Further, $\epsilon = g/R\Omega^2$ is the gravitational excitation made dimensionless by normalization by the centrifugal acceleration $R\Omega^2$, where R is the rotational radius at the beam tip. K is the modal force constant, the dimensionless noise excitation is described as $n(\tau) = N(\tau)/g$ where the noise excitation is normalized by the gravitational excitation, and $\tau = t\omega_0$ is the dimensionless time. Primes stand for derivatives with respect to τ . Finally,

$$\begin{aligned} k_1 &= \lambda^4 - \beta^2 T_l \\ k_3 &= C - \beta^2 T_{nl} \end{aligned} \quad (3.10)$$

are the rotation speed dependent linear and cubic stiffness of the harvester, where λ^4 and C represent the modal linear and cubic stiffness and T_l and T_{nl} the centrifugal acceleration induced tuning factors. For details on the derivation of the factors and the equation as a whole, the reader is referred to the papers by Turhan et al. [24] and Kim et al. [18].

For the system to have a double potential k_1 needs to be negative, this happens when the centrifugal acceleration cancels out the modal linear stiffness of the beam and is seen in the equation as when $\lambda^4 - \beta^2 T_l \leq 0$. The critical buckling frequency where $\lambda^4 - \beta^2 T_l = 0$ then becomes

$$f_{\text{cr}} = \frac{\omega_0}{2\pi} \sqrt{\frac{\lambda^4}{T_l}}. \quad (3.11)$$

All rotations at higher frequencies than the critical buckling frequency will generate a double well potential that is dependent on the rotation speed and have equilibrium positions for the tip at

$$y_{\text{equilibrium}} = \pm L \sqrt{\frac{-k_1}{k_3}}. \quad (3.12)$$

Combining the definitions of k_1 and k_3 in equation 3.10 with equation 3.8 the SR frequency is obtained as

$$f_{\text{SR}} = \omega_0 \frac{(\lambda^4 - \beta^2 T_l) \sqrt{2}}{4\pi} \exp\left(-\frac{(\lambda^4 - \beta^2 T_l)}{4(C - \beta^2 T_{nl})d(\beta)}\right) \quad (3.13)$$

where $d(\beta) = \left(\frac{K\epsilon}{g}\right)^2 D$ using the definitions in equation 3.9. This demonstrates that the SR frequency is dependent on the rotation speed β and by design the harvester

could tune its SR frequency to the rotation speed. When SR occurs the mechanical energy of the harvester will be greatly increased and allows for higher power output.

4. Piezoelectric power generation

Piezoelectric energy harvesting is a popular choice when it comes to power generation on small scales. In this section the basics of the piezoelectric effect, how piezoelectric materials can be used to generate electricity and what is needed to do so will be discussed.

4.1 The Piezoelectric effect

Piezoelectric materials are materials that can be deformed by applying an electric field to it thanks to the piezoelectric property of the material. This effect can also be reversed meaning that by deformation of the material a voltage will be developed. This effect was discovered in 1880 by the brothers Jacques and Pierre Curie [25]. By applying pressure on an electrically neutral crystal the crystal can be deformed which generates a dipole as a result of charge asymmetry in the crystal lattice. Adjacent dipoles tend to align, forming groups of dipoles oriented in the same direction, called Weiss domains. As Weiss domains with different alignment are randomly distributed inside the material there is no electric field present for the summation of all the dipole moments in the material. Using the poling process, which involves applying a strong electric field, the Weiss domains can be arranged in a specific direction giving a permanent polarization of the material [26]. When a mechanical stress is applied to the piezoelectric material a voltage is generated that tries to bring the material back to its original dimensions. Thus, applying electrodes on either side of the piezoelectric material allows for the generated electric charge to be used by creating a passage for the charges to flow [27].

The two main modes used for piezoelectric harvesters is the 31 mode and the 33 mode. The numbers of the mode correspond to the axis that the voltage is generated along and the axis that the stress is applied along. For a beam in the xy-plane these numbers equal $x=1$, $y=2$ and $z=3$. For the 31 mode the voltage is generated along the z axis and the stress is along the x axis. Similarly, the 33 mode generates voltage along the z axis when stress is applied along the z axis. When it comes to cantilever designs such as the one in figure 4.1 the 31 mode is common as the bending of the cantilever will stretch one side of the piezoelectric material and compress the other side. Designing the cantilever with a tip mass allows for generation of large stresses of the piezoelectric materials even for relatively small external forces as well as the possibility for tuning the resonance frequency of the cantilever.

For the setup of the piezoelectric layers in a piezoelectric cantilever the choice stands

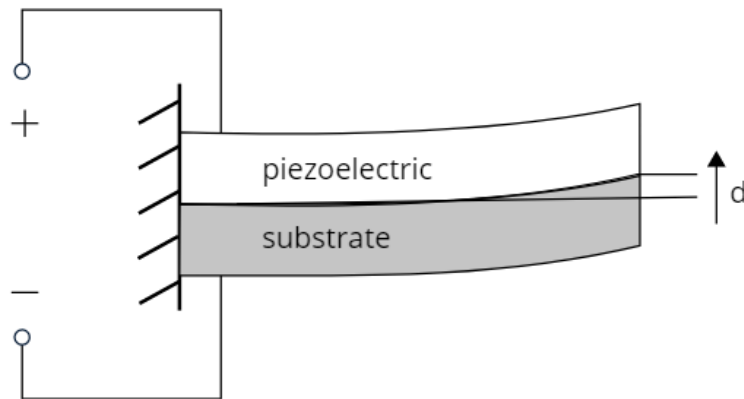


Figure 4.1: Design of a basic piezoelectric cantilever.

between unimorph, as the design in figure 4.1, and bimorph, as seen in figure 4.2. The unimorph consists of only one piezoelectric layer whereas the bimorph consists of two piezoelectric layers in combination with the rest of the beam. For the unimorph the electrodes when used in the 31 mode are simply placed on the top and bottom of the piezoelectric material. For the bimorph, the two layers can be connected either in parallel or in series. The different configurations can be seen in figure 4.2 where the poling of the piezoelectric materials is in opposite direction for the series connected case and in the same direction for the parallel case. The choice of configuration varies from case to case, much dependent on the output specifications [26].

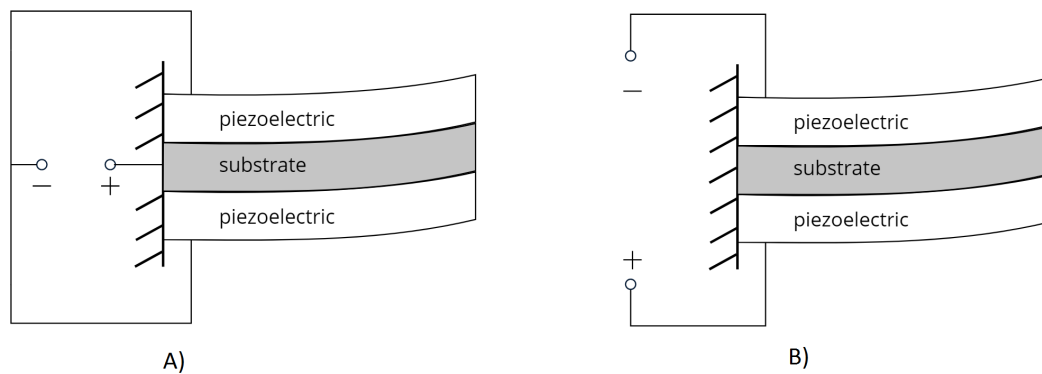


Figure 4.2: Bimorph piezoelectric beams configured in A) parallel and B) series.

4.2 Piezoelectric materials

There are many variables to take into account when it comes to the selection of piezoelectric materials. To mention a few, there is the Q factor, the factor that describes the sharpness of the peak at resonance frequency, with higher Q factor corresponding

to sharper peak. The Curie temperature, the temperature above which the material loses its piezoelectric properties. Moreover, there is the piezoelectric coefficient and coupling coefficient, in the case of energy harvesting these represent the ratio between the electric field that is produced to the mechanical stress applied and the ratio of electric energy accumulated to the mechanical energy applied, respectively [27]. One commonly used piezoelectric material is Lead Zirconate Titanate (PZT) which crystallizes as perovskite crystals giving the material its properties of high piezoelectric coefficient in both the 33 mode and the 31 mode. The crystal structure of PZT is shown in figure 4.3, in the figure it can also be seen that for temperatures above the Curie temperature, T_C , the crystal loses its polarisation.

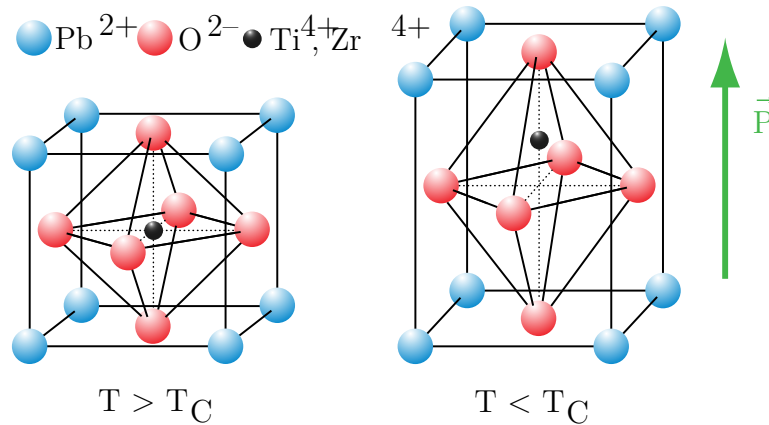


Figure 4.3: Crystal structure of PZT [28].

PZT exists in different versions depending on the composition of the material and is one of the more available piezoelectric materials on the market. Choosing between PZT-5A, PZT-5H and PZT-5J some of the variables mentioned earlier need to be considered. In a paper by W. Hooker the properties of PZT-5A and PZT-5H was tested in a range of temperatures from -150 to 250 °C. The author concluded that PZT-5H had the highest piezoelectric coefficients at room temperature but that it became de-poled at a Curie temperature of 170 °C and thus could not work for higher temperatures. For PZT-5A the Curie temperature lies beyond 250 °C and can therefore work for the entire range of temperatures [29]. PZT-5J was not part of the experiments conducted by W. Hooker but is a hybrid between PZT-5A and PZT-5H giving it a Curie temperature around 250 °C and higher piezoelectric coefficients than PZT-5A according to manufacturer specifications [30]. Comparing with the specifications in section 1.1, PZT-5J would be the best alternative having high piezoelectric coefficients and a large margin from the Curie temperature.

4.3 Power circuit

In section 4.1 it was mentioned that in order to get out electricity from a piezoelectric harvester there needs to be a circuit attached to the piezoelectric element. The circuits allow the current to be manipulated or stored depending on the application. Attaching a simple resistor allows the current to flow, however, this current will

be alternating (AC). As many sensors need direct current (DC) to function the harvester needs to implement a AC-DC converter. One of the most basic AC-DC converters is the full rectifying bridge combined with a capacitance and a resistor as seen in figure 4.4. The components of this circuit are dependent on the piezoelectric material. In order to obtain the best output, the impedance of the circuit and the piezoelectric material needs to match.

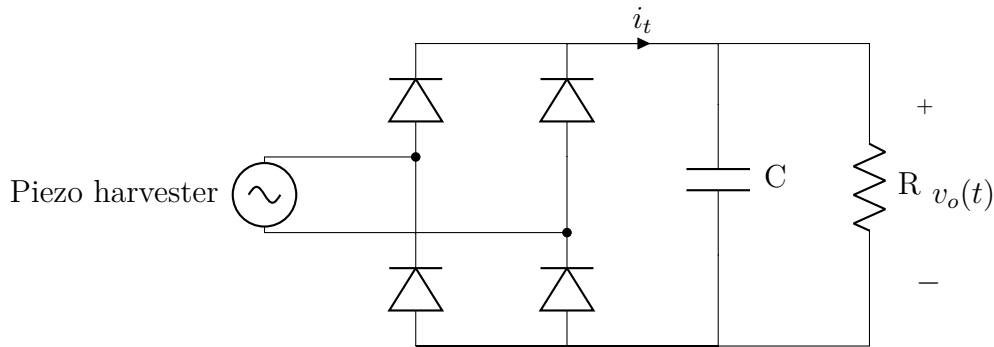


Figure 4.4: Basic power circuit for piezoelectric harvesters.

As the circuit in figure 4.4 is the very basic version of what is needed to get a DC power output from a piezoelectric harvester there are many different alternatives that expands on that circuit to increase the efficiency. Adding a DC-DC converter after the AC-DC converter is an alternative that makes it possible to adjust the output voltage to increase the power generated [31]. Other circuits can also include active elements to increase the efficiency of the circuit.

The design of the power circuit for the harvester is outside the scope of this thesis. However, after the concept is evaluated and if it goes on to become a prototype and possibly a product a power circuit needs to be added for it to be a complete energy harvester.

Part III

Modelling and simulation

During the generation of the concept of this thesis, parts from other concepts and designs were combined to lead up to the goal specifications that is presented in section 1.1. By using the centrifugal force to generate the bistable system needed for stochastic resonance as Kim et al. [18] uses for their harvester, the need for magnets is eliminated as compared to the design by Zhang et al. [16]. Further, by using piezoelectric materials in the same way that Zhang et al. does, the need for coils and magnets as used by Kim et al., to harvest the energy, is removed. So, by combining some of the main parts of these two concepts a design that can be much smaller is proposed. A sketch of the concept is shown in figure 2.2.

In this section the assumptions that are adapted from earlier concepts are discussed, definitions of some new variables are given and parameters for the final design are presented. The numerical simulations, the methods and the programs that are used are explained in the end of the section.

5. Design

As both the harvester designs by Kim et al. [17, 18] and Zhang et al. [16] are made to be placed on the wheels of a car, the assumptions that are used in their concepts need to be examined if they can be applied to a harvester mounted on a flexplate. The first assumption that there is an alternating force on the harvester in the form of alternating gravity stands for a flexplate as well, as long as it is mounted vertically as is the case for cars. The second assumption is that there are noise vibrations within the system. For the concepts where the harvester is mounted on the wheels the noise comes from the rough surface of the ground, however, for the flexplate the noise would come from the engine. The amplitude of the noise is dependent on the revolutions per minute(rpm) of the engine. Some examples on the vibration amplitudes for different rpm for a combustion engine are presented by Burdzik et al. in a paper on vibrations in vehicles [32]. Lastly, the assumption by Kim et al. that the gravitational acceleration is much smaller than the centrifugal acceleration to ensure that the periodic excitation is indeed weak can be obtained on a flexplate as well as the size allows for the harvester to be placed far enough away from the centre of rotation. An example on the size of a flexplate is the Chevrolet flexplate model 12554824, with a diameter of 36 cm [33]. Kim et al. also mentions the fact that the noise from the road only acts in one direction and thus needs to be amplitude modulated by the factor $\sin(\Omega t)$ as well and the authors' presents an analysis showing that even for modulated noise the assumptions used still stands. This does not apply in the case of the application on the flexplate as there are vibrations in multiple directions in an engine as can be seen in the paper by Burdzik et al. [32]. If the vibrations turn out to be much larger in one direction the modulated version can be used.

5.1 Redefining variables

As the assumptions still stand for the application on a flexplate the next step is to design the harvester with the given specifications. As the equation 3.9 is based on the form of a homogeneous beam and piezoelectric energy harvesters consist of multiple materials stacked on top of each other along the beams length the moment of inertia will need to be altered. To get the effective moment of inertia for the harvester beam the methods for the first mode approximation by Shafer et al. are implemented [34]. Defining the variables

$$\eta = \frac{E_p}{E_s} \tag{5.1}$$

$$\kappa_p = \frac{2t_p}{t} \tag{5.2}$$

where E_p and E_s stands for the Young's modulus along the beam length for the piezoelectric and the substrate and t_p and t is the thickness of the piezoelectric

material and the entire beam. The factor 2 comes from the assumption that the beam has a bimorph design, one piezoelectric layer on each side of the substrate, to make the beam symmetric. Using these definitions and having w as the width of the beam, the effective moment of inertia becomes

$$I_{\text{eff}} = \frac{wt^3}{12} \left((\eta - 1)\kappa_p^3 - 3(\eta - 1)\kappa_p^2 + 3(\eta - 1)\kappa_p + 1 \right) \quad (5.3)$$

for a beam entirely made of the substrate material but that has the same stiffness as the harvester beam. This allows for the substrate's Young's modulus, E_s , to be used for the entire harvester. With the reworked variables the multilayer harvester can be used in calculations as a homogeneous beam.

5.2 Harvester parameters

To streamline the evaluation of the concept the design of the harvester was chosen to be based on a commercially available piezoelectric cantilever beam. With the physical dimensions of the harvester stated as in table 5.1, the variables remaining to be defined are the weight of the proof mass and the radius of rotation. The configuration of these variables was varied during the numerical simulations to optimize the power output. The dimensions and values of the harvester are given in table 5.1 as Harvester 1. The harvester is 18 mm longer and 0.8 mm wider than the goal specifications. However, it can still give an estimation how well a harvester within the goal specification could perform experimentally without the need for a specially designed and produced harvester. This can greatly reduce the cost and time needed for the evaluation of the concept. The commercial harvester used in this thesis has a working temperature range of -60 to 120 °C, thus the PZT is not the limiting factor when it comes to temperature, but the epoxy used between the layers is. This range can be increased in a final design by using a different epoxy.

Table 5.1: Energy harvester parameters used in simulations.

Parameters	Harvester 1
Beam dimension (L×W×t)	58×6.8×0.7 mm ³
Piezo dimension (L×W×t)	58×6.8×0.25 mm ³
Weight (proof mass/total)	5/6.1 g
Young's modulus (Piezo/Substrate)	5.2/2.6 GPa
Density (Piezo/Substrate)	7800/1900 kg/m ³
Radius of rotation	40 mm

6. Solving the equation of motion in MATLAB

To solve the differential equation 3.9, it is reworked from a second-order differential equation into a system of first-order differential equations by using a change of variables. Let $q(\tau) = Q_1$ and $\frac{dq}{d\tau} = Q_2$ and equation 3.9 can be rearranged as

$$\frac{dQ_1}{d\tau} = Q_2 \quad (6.1)$$

$$\frac{dQ_2}{d\tau} = -2\zeta\lambda^4 Q_2 - k_1 Q_1 - k_3 Q_1^3 + K\epsilon n(\tau) + K\epsilon \sin(\beta\tau). \quad (6.2)$$

This system can then be solved numerically by using the standard solver, ODE45, in MATLAB. ODE45 uses a Runge-Kutta method and takes the input of time span and initial conditions of the vector that is solved for, Q_1 and Q_2 in this case [35]. The dimensionless output of the harvester is then given by the dimensionless version of equation 3.4 that is given by

$$P_{\text{avg}} = \zeta_e \langle Q_2^2 \rangle. \quad (6.3)$$

The simulation results based on equation 6.3 and table 5.1 are presented in section 9.2.

7. Numerical simulations in COMSOL

To compare the power output that is calculated using the equation of motion, a model was created in COMSOL Multiphysics. COMSOL is a physics based Finite Element Analysis tool that covers many different fields and allows for evaluation of concepts and designs using cross-disciplinary physics modules. The basics of COMSOL and how to work with the program is covered in the book "*Multiphysics Modeling Using COMSOL*" by Roger W. Pryor [36]. The workflow follows a sequential path making the process of designing and determining boundary conditions, running and analyzing the result easier to customize depending on what is needed of the simulation.

In this section the basics that were used when designing the harvester in COMSOL will be presented, starting with the creation of the geometry, definition of the boundary conditions and ending with the study steps and visualization of the results.

7.1 Geometry

As the harvester of the concept was based on a commercial harvester the dimension was already fixed. The values for Harvester 1 in table 5.1 were recreated in COMSOL in 3D using the built-in block structures. On the end of the harvester a proof mass was added in the form of two blocks, one on each side of the harvester for symmetry. The finished design of the harvester can be seen in figure 7.1. In this step the electrodes of the commercial harvester, that are made of copper and have a thickness of $30\ \mu\text{m}$ each were neglected.

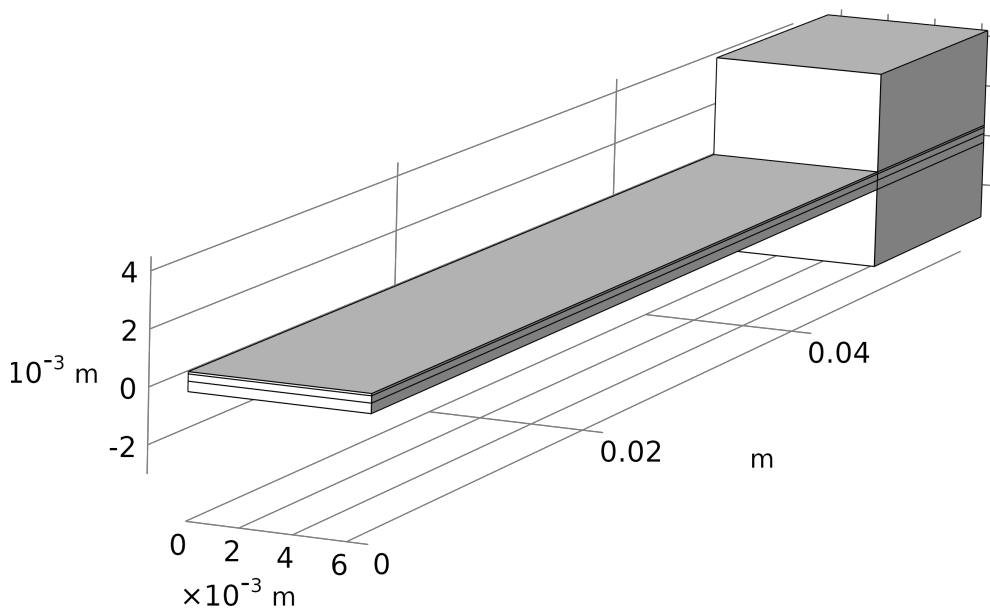


Figure 7.1: Harvester model in COMSOL.

7.2 Materials

After the creation of the geometry the material of each part needed to be defined. This was done using the built-in material library with small modifications for the properties to match with the data from the manufacturer also stated in table 5.1. The proof mass was set to the same material as the substrate of the beam but had the density modified in order to easily vary the mass and obtain the mass that was needed.

7.3 Boundary conditions

With the geometry and materials set the next step is to establish the boundary conditions. The boundary conditions define the constraints on the system that make for the simulations to replicate the reality as accurately as possible. The

boundary conditions are divided into two main parts for piezoelectric simulations in COMSOL: Solid Mechanics and Electrostatics.

7.3.1 Solid Mechanics

A **Fixed Constraint** was placed on the end of the harvester that does not have the proof mass, simulating a clamping to a fixed structure. The rest of the harvester was given a **Prescribed Acceleration** in terms of g and for the substrate a **Damping** was added to tune the displacement at resonance and eliminate unreasonable bending.

7.3.2 Electrostatics

For the electrostatic conditions only the piezoelectric parts of the geometry were needed. On the top and bottom of the piezoelectric layer a **Ground** and a **Terminal** were added as the electrodes and connected with an impedance with the value R_{load} . The value of R_{load} was determined by sweeping over different loads and finding the peak output. Further, the piezoelectric layer was given **Charge Conservation** and the initial value 0 for the ground.

With all the boundary conditions set the multiphysics module combined the conditions from **Solid Mechanics** and **Electrostatics**, allowing the piezoelectric effect to be simulated.

7.4 Mesh

The mesh is a very important part of the simulation as a well-defined mesh gives more precise results. However, a finer mesh also requires significantly more computing power and memory to be solved for. Applying a finer mesh on the critical parts such as the piezoelectric material and a rougher mesh on parts such as the proof mass allows for less demanding calculations and still gives good results. This was achieved by using the **Finer** settings for the mesh on the piezoelectric material, seen as blue in figure 7.2, the **Rough** setting on the proof mass and **Normal** setting for the substrate as it is not as critical as the piezoelectric material.

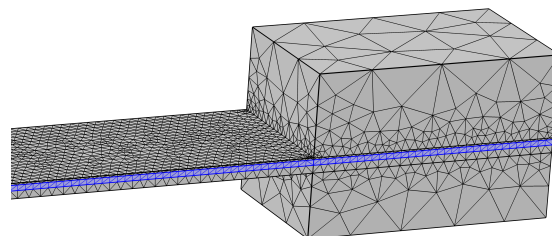


Figure 7.2: The mesh outline of the model in COMSOL, PZT-5J shown in blue.

7.5 Study steps

For the simulation of the system the main studies that were used was the **Eigenfrequency** study and the **Frequency Domain**. The **Eigenfrequency** study gave the resonance frequencies of the harvester and the mode shapes for them. This limited the frequencies that needed to be swept when using the **Frequency Domain** to analyze the power output and the matching impedance.

7.6 Visualization of results

After the studies are completed the results need to be visualized. Most of the results were best presented in simple line plots, however also the surface plot function was used to visualize the mode shape of the harvester. The simulation results obtained with COMSOL are presented in section 9.1.

Part IV

Experiments

For the experimental part of the project the goal included experimental extraction of the matched resistance for maximum power generation, the damping ratio of the harvester and measurements for comparison with the theoretical bending of the harvester. With these goals in mind the experimental part can be divided into three parts: Frequency and resistance sweeps, damping and buckling. The experimental results are presented in section 9.1.

8. Method

During the frequency and resistance sweeps a Miniature Electrodynamic Shaker from the Modal Shop (Model 2007E), driven by a SmartAmp power amplifier by Agilent (Model 2100E21-100) was used to generate a sinusoidal excitation for the harvester. The response of the harvester was recorded using both an oscilloscope by PicoTechnology (Picoscope 2000 series) to measure the output voltage and a laser distance sensor by Panasonic (HL-G1 measurement sensor) to measure the displacement of the harvester. The experiments were set up as seen in figure 8.1 with the oscilloscope connected to a computer to simplify the extraction of data.

For the bending measurements the force was measured using a simple setup: an EKS Electronic Scale with the setup in figure 8.2. The goal was to compare the bending of the harvester to the theoretical calculations used in the simulations when a force equivalent to the centrifugal force is applied to the harvester. Finally, the harvester was placed in a rotating system with the proof mass facing inwards as seen in figure 8.3. The motor used to drive the rotation was a DC motor from Micro Motors (RH158 12V) and pictures of the harvester during the tests was taken with a digital camera from Nikon (D5300).

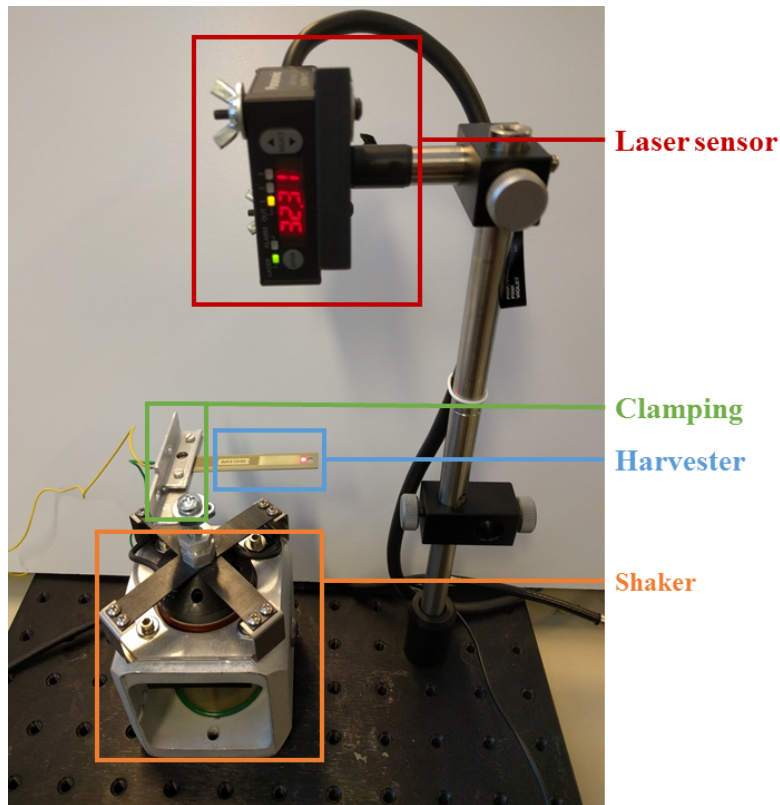


Figure 8.1: Experimental setup for frequency and resistance sweeps.

8.1 Frequency and resistance sweeps

The resonance frequency of the harvester was found by sweeping over a range of frequencies with an open circuit and locating the output and displacement peak in the spectrum. It was valuable to measure both displacement and voltage as they could validate each other and eliminate possible errors.

As the generated power of the harvester is strongly dependent on the resistance in the circuit it is important that the right resistance is used. By performing a resistance sweep at the resonance frequency the matching impedance can be found and compared with the value obtained in COMSOL. Experimentally the sweep is done by measuring the voltage at the resonance frequency and changing the resistance in the circuit and the generated power is then given as $P = \frac{V_{\text{rms}}^2}{R}$. As the measured voltage is peak to peak it is transformed as $V_{\text{rms}} = \frac{V_{\text{ptp}}}{\sqrt{2}}$ before the power calculations. Comparisons with an open and a closed-circuit voltage is also done as to validate the measurements.

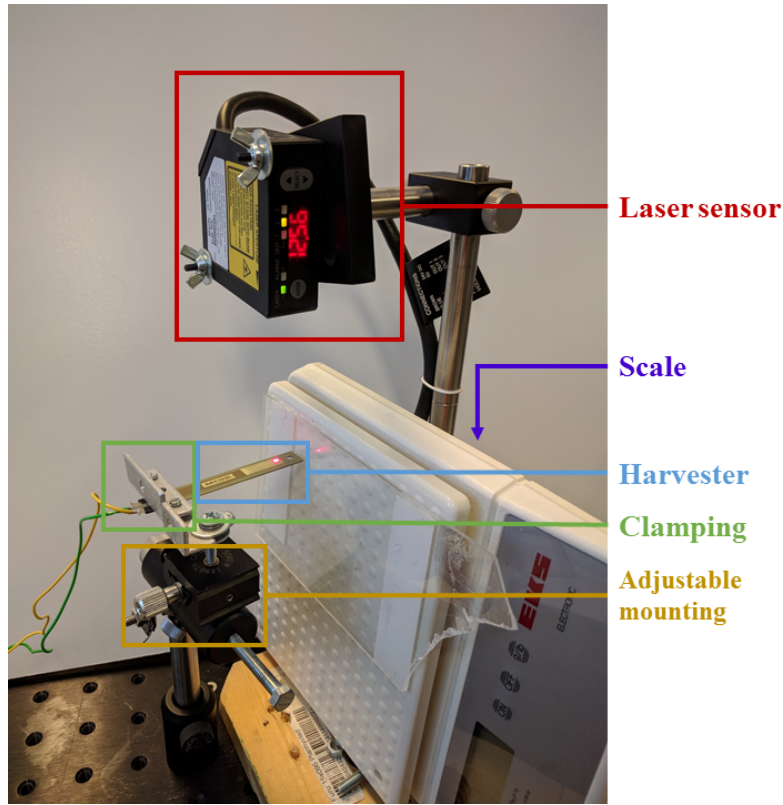


Figure 8.2: Experimental setup for the static buckling experiment with the harvester mounted on an adjustable setup in order to apply force.

8.2 Damping

The damping ratio, ζ is calculated using the time dependent tip displacement and measuring the displacement peaks as

$$\zeta = \frac{\delta}{\sqrt{4\pi^2 + \delta^2}} = \frac{\frac{1}{j} \ln \frac{X_i}{X_{i+j}}}{\sqrt{4\pi^2 + \frac{1}{j} \ln \frac{X_i}{X_{i+j}}}} \quad (8.1)$$

where δ is the logarithmic decrement, j is the number of sampling points, X_i and X_{i+j} is the displacement peak for the first and the last sampling point [37]. The logarithmic decrement is defined as the natural logarithm of the ratio of two following peaks [38]. For systems with low damping or with high uncertainty of the peaks, a higher number of sampling points between the peaks used in the ratio can give clearer results.

The damping ratio can be divided into pure mechanical damping ratio, ζ_m , and electrical damping ratio, ζ_e , as $\zeta = \zeta_m + \zeta_e$. The calculated damping ratio can be approximated as the pure mechanical damping ratio for the case where no external circuit is attached.

For the measurements of the electrical damping ratio, ζ_e , a resistor is connected to the harvester. The circuit in combination with the piezoelectric material generates an electrically induced damping beyond the pure mechanical damping. Using both these measurements ζ_e can be extracted [37].

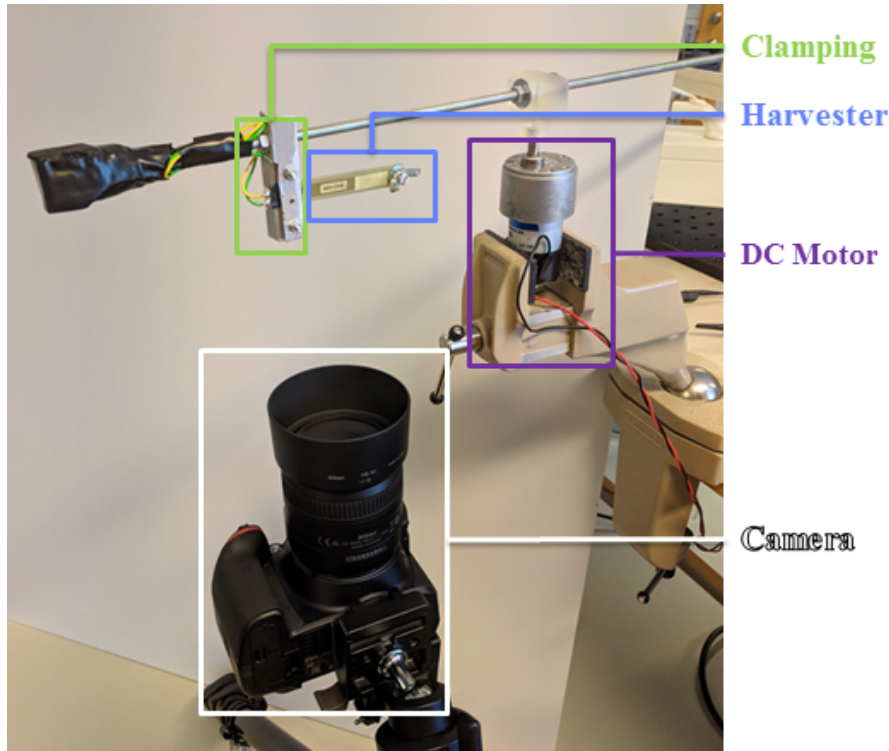


Figure 8.3: Experimental setup for rotation testing in the horizontal configuration.

8.3 Buckling

The deformation of the harvester under the influence of the centrifugal force is represented by using an equivalent force in a static environment, as shown in figure 8.2 and measuring the displacement using the laser distance sensor. The force applied to the harvester is calculated as $F_c = m_{\text{tip}}\omega^2(R - L_{\text{beam}})$. The critical force when the buckling occurs is also compared to the equivalent force where $\omega = f_{CR}$ from equation 3.11. When the centrifugal force acts on the harvester the proof mass is entirely free to move, in the static experiment seen in figure 8.2 the end of the harvester cannot be counted as free as the tip is fixed in translation by the friction of the scale. Instead, the end can be seen as a mix between a free end and an end where the translation is fixed, and the rotation is free. Comparing the two cases gives that the measurement can be seen as an upper limit for the force needed to buckle a free beam as a beam that is fixed in translation and free in rotation has a buckling force 8 times as large as a free beam according to Euler's critical load [39]. The bending of the harvester was also tested in a rotating system, as seen in figure 8.3, to see if the centrifugal force could generate buckling and to mimic the actual application for the harvester.

Part V

Results and Discussion

In part III and part IV, the simulations, experiments and measurement methods were described. In this part, the data obtained from the simulations and the measurements for the experiments will be presented. Further, the results as well as the concept as a whole will be discussed and evaluated. Lastly, possible next steps for the development of the concept are proposed.

9. Results

The experiments were performed in large to validate some of the assumptions made in the simulations, as well as to get experimental values of the specific harvester that was used. In section 9.1 the results of the experiments are set against the corresponding results of the simulations and the obtained data that is used in the equation of motion simulation is presented. In section 9.2 the results of the movement of the harvester as well as the power output as derived from the equation of motion simulation are displayed.

9.1 Experimental and COMSOL

The resonance frequency of the harvester without proof mass was measured to be 46 Hz, comparable with the value of 49 Hz given by the manufacturer. In COMSOL the resonance frequency was 67 Hz. The resistance sweeps that was performed at resonance both in COMSOL and experimentally are shown in figure 9.1, with the peak power at approximately 70 k Ω in both cases.

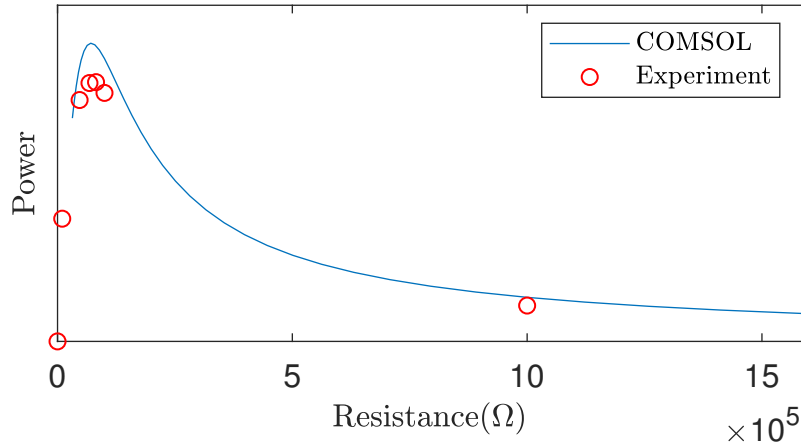


Figure 9.1: The resistance sweeps in COMSOL and experimental showing the power at resonance dependent on resistance of a harvester without proof mass.

The total damping ratio, ζ , was calculated to be 0.0145 and the mechanical damping ratio, ζ_m , to be 0.0104 using the experimental measurements. This gives the electrical damping ratio, $\zeta_e = 0.0041$. One of the damping tests are shown in figure 9.2 where the peaks is marked in red. These values were then used for the simulations in order to replicate the harvester as accurately as possible.

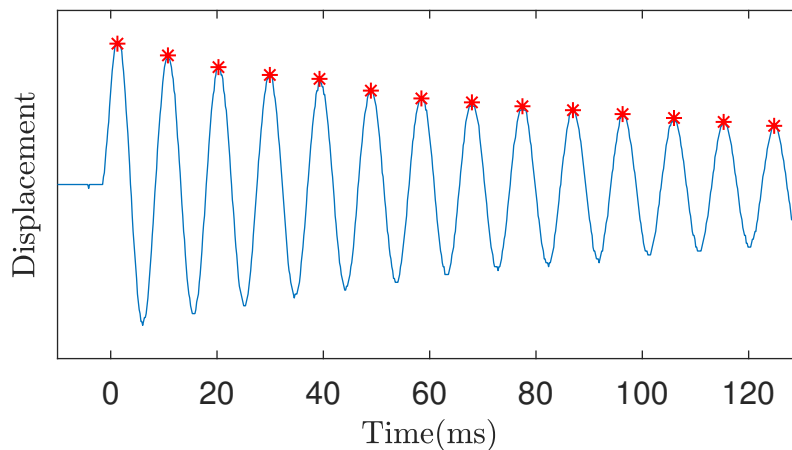


Figure 9.2: Displacement over time of the harvester with the peak positions marked for use in damping calculations.

The theoretical values for the equilibrium positions as a function of rotation frequency, based on equation 3.12, is shown in figure 9.3 where the critical buckling

frequency is seen at 3 Hz. In figure 9.4 the experimental data of the buckling frequency is shown in red, the calculated lower limit of the buckling frequency in green and the displacement at specific rotation speeds is shown in blue. The experimental displacement of the beam has increasing error margins with the rotation speed due to a too simple measurement setup.

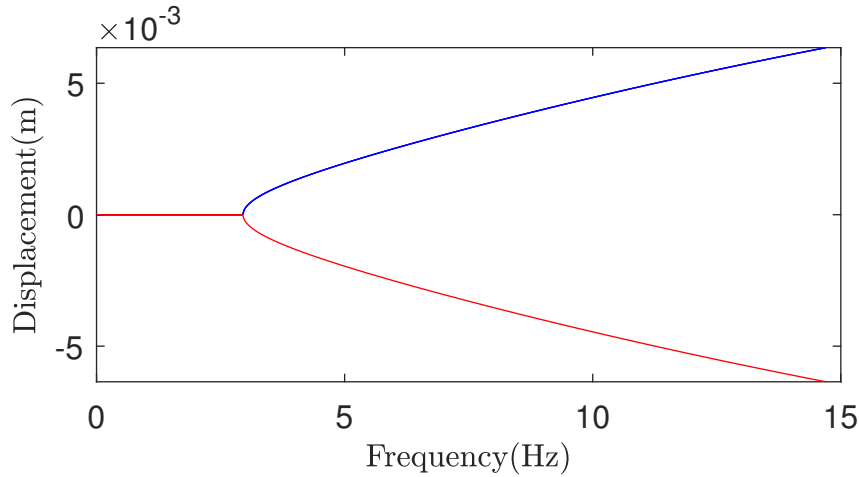


Figure 9.3: The equilibrium positions of the double potential as a function of rotation frequency. The critical buckling frequency is seen at 3 Hz, where the system becomes bistable.

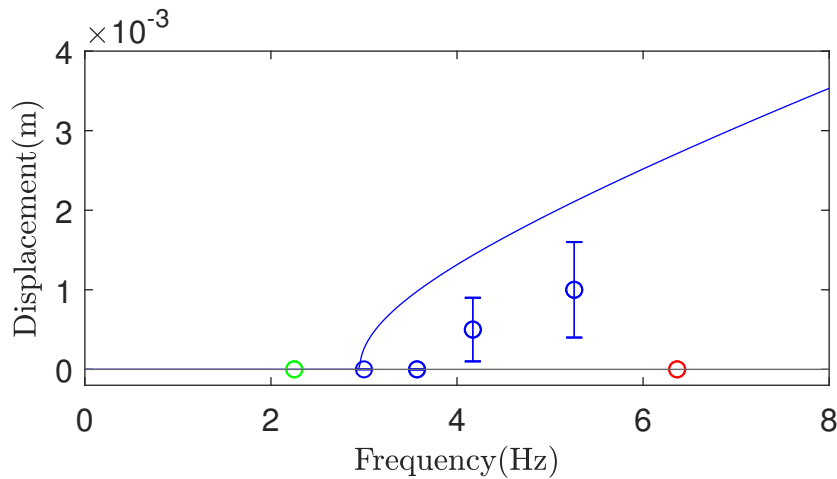


Figure 9.4: Theoretic bending of the harvester with experimental bending added as blue circles, the experimental buckling frequency as red and the calculated lower limit of buckling frequency as green.

The power output of the harvester at specific peak-to-peak displacements could only be done for low frequencies in displacement experiments and is compared in table 9.1 with the power output given in COMSOL for matching displacement and frequency. The peak-to-peak displacement was chosen as the setup limited the choice of displacement. The frequency 11 Hz is added in COMSOL as it is the frequency

where the equilibria are 5 mm from the zero point. The last two rows of the table are added to compare with the output obtained in section 9.2.

Table 9.1: Power output at specific peak-to-peak (ptp) displacement for different frequencies.

f(Hz)	ptp(m)	P(μ W), COMSOL	P(μ W), Experiments
1	0.01	26.1	12.3
2	0.01	66.0	65.6
3	0.01	92.3	114.5
11	0.01	367.5	-
11	0.03	3000	-

9.2 Equation of motion simulation

The results of the numerical solution for the equation of motion, equation 3.1, is visualized in the following figures. In figure 9.5 the displacement of the harvester's endpoint is plotted over time for the case of only alternating gravity and the case of both alternating gravity and white noise. In this figure, the movement between the two stable positions occurs for the case with white noise but not for the case without. In figure 9.6 and figure 9.7 the velocity of the end point is plotted against its displacement, again for the cases without and with white noise respectively. Figure 9.7 shows a case with stochastic resonance where all movement is between the two stable position and no interwell movement.

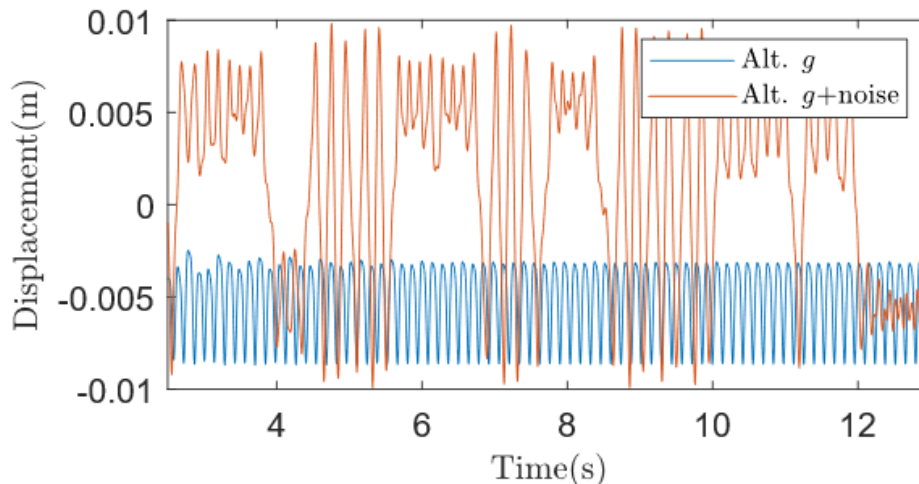


Figure 9.5: Simulation of the displacement over time of the tip of the harvester under the cases: only alternating gravity and alternating gravity and added white noise.

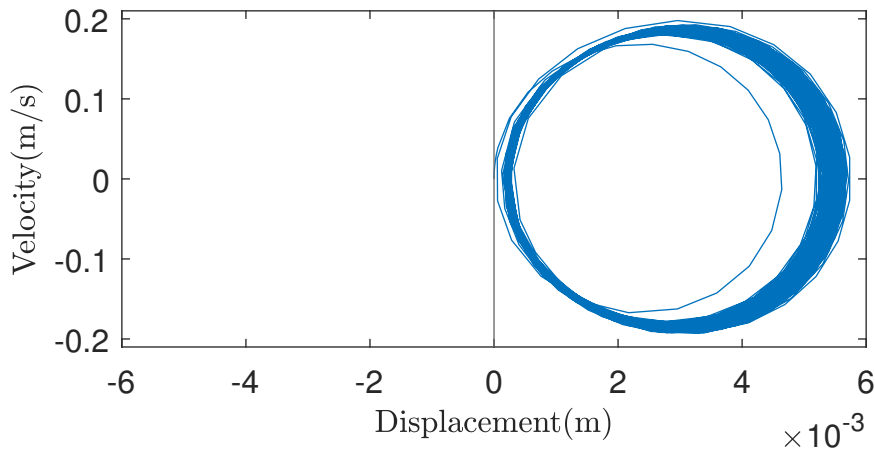


Figure 9.6: The velocity as a function of displacement for the proof mass when only excited by alternating gravity.

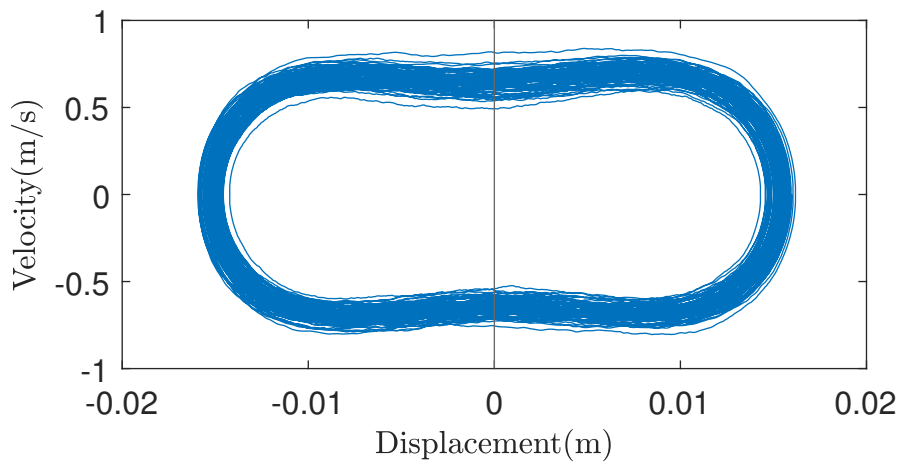


Figure 9.7: The velocity as a function of displacement for the proof mass when SR occurs under excitation by alternating gravity and white noise.

Finally, the simulations for power as a function of rotation frequency is presented in figure 9.8. The figure is an average of multiple runs as the occurrence of SR is dependent on white noise and thus is random. The figure shows a peak output of $370 \mu\text{W}$ and a bandwidth of 2.44 Hz , corresponding to a bandwidth of 146.4 rpm .

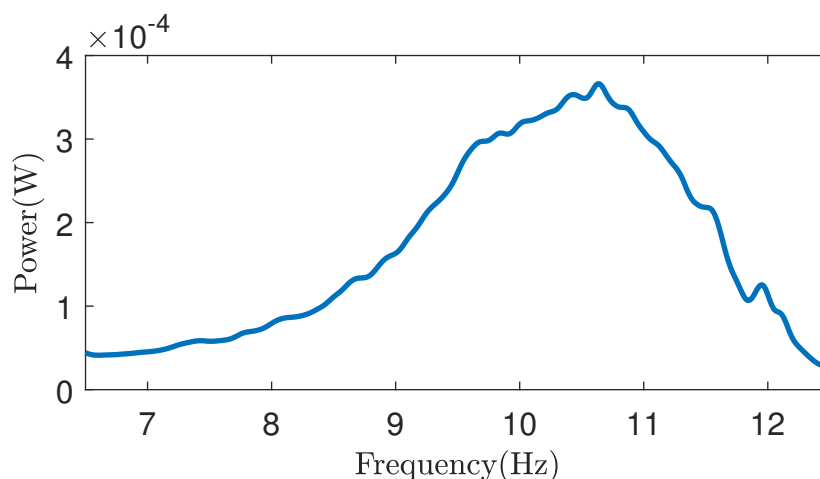


Figure 9.8: The power output as a function of rotation frequency showing a peak power of $370 \mu\text{W}$ and a bandwidth at 3 dB of 2.44 Hz.

A comparison of the bandwidth obtained in figure 9.8 with the bandwidth of a similar harvester with the resonance frequency at 10.6 Hz that does not use SR and have the same Q-factor as the harvester used in the simulation is shown in figure 9.9. The Q-factor is obtained as $Q = \frac{1}{2\zeta}$, with ζ from the damping measurements. The power of the comparing harvester is normalized to match the power obtained in the simulations.

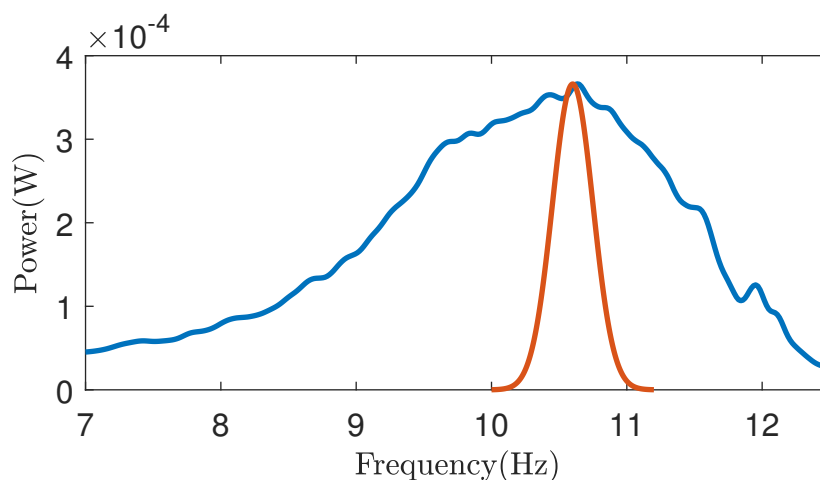


Figure 9.9: Bandwidth comparison between the concept harvester and a harvester with the same Q-factor as obtained from the measured damping ratio.

10. Discussion

The simulations done on the COMSOL model demonstrated a close resemblance to the real harvester when compared with the experimental data. The matching resistances for the harvesters were very close, seen in figure 9.1, and the power output for the same displacement at low frequencies reflected a similar behaviour. The largest difference between the COMSOL model and the real harvester seems to be the unloaded resonance frequency where the harvester was measured to have its resonance frequency at 46 Hz whereas the COMSOL model has its resonance frequency at 67 Hz. This difference can likely be explained by the boundary conditions used in COMSOL. When using the **Fixed Constraint** in Solid Mechanics the boundary that is fixed is totally fixed. In comparison the real harvester is clamped, allowing the material at the clamping to interact in the bending as well. This would make the model in COMSOL stiffer in comparison and thus have a higher resonance frequency.

The experimental results of the bending indicate that the bending will indeed occur over a specific threshold. The reason it did not follow the theoretical prediction more precisely can have many explanations. The setup had some shortcomings when it came to the stability of the mounting of the harvester making the risk of misalignment prominent, something that could affect the results. When mounting the harvester on a flexplate this problem could be eliminated as the flexplate itself could work as a guiding plane. The measurements also imply that the estimation made in section 8.3 that the force measured in the static environment could be used as an upper limit for the buckling frequency holds, as both the theoretical value and the frequency of bending in the rotational test is within the span that was estimated. This can be seen in figure 9.4 where the measured upper limit is in red and the calculated lower limit is in green.

With the presence of a double potential as generated by the buckling of the harvester the difference in movement when comparing movement inside one potential well and movement between the potentials wells is significant. When comparing the results in figure 9.6 and 9.7 the top velocity is not only increased but also kept during a longer time as the distance is significantly increased as well. As the instantaneous power is dependent on the velocity squared there is no doubt that the occurrence of SR can increase the mechanical power available in a system.

The power output for a set peak-to-peak displacement and different frequencies could only be done for low frequencies because of limitations in the experimental setup. The experiments did however match well with the simulations done in COMSOL where higher frequencies could be simulated. When comparing the power output of a set displacement at resonance frequency in COMSOL with the power output estimated using the equation of motion, with the same displacement and frequency, the COMSOL model gives higher output. This is expected as during SR some of the energy is spent when passing the potential barrier. This can be seen in figure 9.7 where the velocity is actually in a local minimum at zero displacement as this represents the top of the potential barrier. Another reason that COMSOL is giving

higher output can be that the damping ratio is assumed to be constant for the harvester in the equation of motion. For larger deformation the electrical damping can potentially increase as the stress on the piezoelectric material increases, however, this would need further experiments to validate.

The harvester performs the best in the range of 9.22 to 11.66 Hz or 553 to 700 rpm. This is rather low numbers considering that many engines run at order of up to thousands rpm. As the harvester used for the simulations was based on an off the shelf harvester the ranges that it could be designed to work became limited. However, this does not mean that a harvester based on this concept cannot work at those levels given the right design.

The electrical damping ratio, ζ_e , was measured to be 0.0041. Compared with a similar piezoelectric harvester by Huang et al., with almost the same dimensions but with a bimorph configuration that has $\zeta_e = 0.012$ it is clear that it is an area that could be improved in further iterations [37].

10.1 Future work

With the simulations indicating good performance from an off the shelf harvester using the concept that is proposed and experiments that point towards the base assumptions being fulfilled, the next step would be to recreate the environment that was used to test the harvester in a real rotating system with large vibrations. Given such a setup the experiments can show if stochastic resonance does occur as predicted or not. If experimental verification is accomplished the next step would be to move on to the specific application that the concept is aimed at. This would include mapping the vibrations of the flexplate. The information of the vibrations would allow for a more precise design of the harvester when used in combination with a desired operation rpm.

During this design phase other arrangements of the piezoelectric material and the substrate could also be evaluated. A stiffer substrate could allow for operation at high rpm without risking breaking the piezoelectric material and a bimorph configuration could allow for higher power output. Working towards a functional harvester a power circuit needs to be made and implemented together with the harvester.

Part VI

Conclusion

In this thesis a concept has been generated, eliminating the need of magnets and coils, which led to a reduced size compared to the two designs it was based on. This made the new design more suitable for the specific application. The results of the simulations of this thesis shows that the concept that was generated has potential to work as a harvester for a sensor mounted on a flexplate. The simulated result of a peak power output of $370 \mu\text{W}$ and a bandwidth of 2.44 Hz using a commercially available harvester is a good base and further development in the design could improve the performance of the harvester.

The experiments of the thesis were rather simple in the setup and had quite large limitations. Thus, there are still more work to do experimentally to validate the simulations. Next, a mapping of the vibrations is needed in order to see if the simulations predict stochastic resonance in the actual system.

References

- [1] Alliedmarketresearch.com. *Sensor Market by Type, Global Opportunity Analysis and Industry Forecast, 2014 - 2022*. 2016. URL: www.alliedmarketresearch.com/sensor-market (visited on 04/23/2019).
- [2] Shantanu Bhattacharya et al. *Sensors for Automotive and Aerospace Applications*. Springer, 2018.
- [3] Huicong Liu et al. “A comprehensive review on piezoelectric energy harvesting technology: Materials, mechanisms, and applications”. In: *Applied Physics Reviews* 5.4 (2018), p. 041306.
- [4] Alessandro Giuliano, Vlad Marsic, and Meiling Zhu. “Implementation and testing of an elastic strain powered wireless sensing system for energy-autonomous applications”. In: *2012 IEEE International Conference on Green Computing and Communications*. IEEE. 2012, pp. 681–684.
- [5] Steven W Arms et al. “Tracking pitch link dynamic loads with energy harvesting wireless sensors”. In: *ANNUAL FORUM PROCEEDINGS-AMERICAN HELICOPTER SOCIETY*. Vol. 63. 2. AMERICAN HELICOPTER SOCIETY, INC. 2007, p. 934.
- [6] Fumio Narita and Marina Fox. “A review on piezoelectric, magnetostrictive, and magnetoelectric materials and device technologies for energy harvesting applications”. In: *Advanced Engineering Materials* 20.5 (2018), p. 1700743.
- [7] Heung Soo Kim, Joo-Hyong Kim, and Jaehwan Kim. “A review of piezoelectric energy harvesting based on vibration”. In: *International journal of precision engineering and manufacturing* 12.6 (2011), pp. 1129–1141.
- [8] J Xu and J Tang. “Multi-directional energy harvesting by piezoelectric cantilever-pendulum with internal resonance”. In: *Applied Physics Letters* 107.21 (2015), p. 213902.
- [9] Haifeng Zhang and Karim Afzalul. “Design and analysis of a connected broadband multi-piezoelectric-bimorph-beam energy harvester”. In: *IEEE transactions on ultrasonics, ferroelectrics, and frequency control* 61.6 (2014), pp. 1016–1023.
- [10] Agin Vyas et al. “A Micromachined Coupled-Cantilever for Piezoelectric Energy Harvesters”. In: *Micromachines* 9.5 (2018), p. 252.
- [11] Qi Wang et al. “High power density energy harvester with high permeability magnetic material embedded in a rotating wheel”. In: *Nondestructive Characterization for Composite Materials, Aerospace Engineering, Civil Infrastructure, and Homeland Security 2012*. Vol. 8347. International Society for Optics and Photonics. 2012, p. 83470V.
- [12] Ming Li et al. “A rotation energy harvester employing cantilever beam and magnetostrictive/piezoelectric laminate transducer”. In: *Sensors and Actuators A: Physical* 166.1 (2011), pp. 102–110.
- [13] Mingjie Guan and Wei-Hsin Liao. “Design and analysis of a piezoelectric energy harvester for rotational motion system”. In: *Energy Conversion and Management* 111 (2016), pp. 239–244.

-
- [14] Lei Gu and Carol Livermore. “Passive self-tuning energy harvester for extracting energy from rotational motion”. In: *Applied Physics Letters* 97.8 (2010), p. 081904.
- [15] M Löhndorf et al. “Evaluation of energy harvesting concepts for tire pressure monitoring systems”. In: *Proceedings of Power MEMS* (2007), pp. 331–334.
- [16] Y Zhang et al. “Broadband vibration energy harvesting by application of stochastic resonance from rotational environments”. In: *The European Physical Journal Special Topics* 224.14-15 (2015), pp. 2687–2701.
- [17] Hongjip Kim, Wei Che Tai, and Lei Zuo. “Self-tuning stochastic resonance energy harvester for smart tires”. In: *Active and Passive Smart Structures and Integrated Systems XII*. Vol. 10595. International Society for Optics and Photonics. 2018, 105950U.
- [18] Hongjip Kim et al. “Self-tuning stochastic resonance energy harvesting for rotating systems under modulated noise and its application to smart tires”. In: *Mechanical Systems and Signal Processing* 122 (2019), pp. 769–785.
- [19] Roberto Benzi, Alfonso Sutera, and Angelo Vulpiani. “The mechanism of stochastic resonance”. In: *Journal of Physics A: mathematical and general* 14.11 (1981), p. L453.
- [20] Luca Gammaitoni et al. “Stochastic resonance”. In: *Reviews of modern physics* 70.1 (1998), p. 223.
- [21] Bruce McNamara and Kurt Wiesenfeld. “Theory of stochastic resonance”. In: *Physical review A* 39.9 (1989), p. 4854.
- [22] CR McInnes, DG Gorman, and Matthew P Cartmell. “Enhanced vibrational energy harvesting using nonlinear stochastic resonance”. In: *Journal of Sound and Vibration* 318.4-5 (2008), pp. 655–662.
- [23] Peter Hänggi, Peter Talkner, and Michal Borkovec. “Reaction-rate theory: fifty years after Kramers”. In: *Reviews of modern physics* 62.2 (1990), p. 251.
- [24] Özgür Turhan and Gökhan Bulut. “On nonlinear vibrations of a rotating beam”. In: *Journal of sound and vibration* 322.1-2 (2009), pp. 314–335.
- [25] Shaul Katzir. “The discovery of the piezoelectric effect”. In: *THE BEGINNINGS OF PIEZOELECTRICITY*. Springer, 2006, pp. 15–64.
- [26] Thorsten Hehn and Yiannos Manoli. “Piezoelectricity and energy harvester modelling”. In: *CMOS Circuits for Piezoelectric Energy Harvesters*. Springer, 2015, pp. 21–40.
- [27] SO Reza Moheimani and Andrew J Fleming. *Piezoelectric transducers for vibration control and damping*. Springer Science & Business Media, 2006, pp. 9–35.
- [28] Pinin. *Perovskite*. 2010. URL: <https://upload.wikimedia.org/wikipedia/commons/9/9a/Perovskite.svg> (visited on 05/14/2019).
- [29] Matthew W Hooker. “Properties of PZT-based piezoelectric ceramics between-150 and 250 C”. In: (1998).
- [30] Steminc. *Piezo Material Properties*. URL: <https://www.steminc.com/PZT/en/piezo-materials-properties> (visited on 05/07/2019).
- [31] Geoffrey Ottman et al. “Adaptive piezoelectric energy harvesting circuit for wireless, remote power supply”. In: *19th AIAA Applied Aerodynamics Conference*. 2002, p. 1505.

- [32] Rafał Burdzik and Radovan Doleček. “Research of vibration distribution in vehicle constructive”. In: *Perner’s Contacts 7.4* (2012), pp. 16–25.
- [33] chevrolet.com. *Small-block Flywheels and Flexplates*. 2019. URL: <https://www.chevrolet.com/performance/components/small-block-engines/flywheels-flexplates> (visited on 05/06/2019).
- [34] Michael W Shafer, Matthew Bryant, and Ephraim Garcia. “Designing maximum power output into piezoelectric energy harvesters”. In: *Smart Materials and Structures* 21.8 (2012), p. 085008.
- [35] Nur Adila Faruk Senan. “A brief introduction to using ode45 in MATLAB”. In: *University of California at Berkeley, USA* (2007).
- [36] Roger W Pryor. *Multiphysics modeling using COMSOL®: a first principles approach*. Jones & Bartlett Publishers, 2009.
- [37] Hualin Huang et al. “Elastic and electric damping effects on piezoelectric cantilever energy harvesting”. In: *Ferroelectrics* 459.1 (2014), pp. 1–13.
- [38] André Preumont. *Vibration control of active structures*. Vol. 2. Springer, 1997.
- [39] Hans Lundh. *Grundläggande hållfasthetslära*. Institutionen för hållfasthetslära, Tekniska högsk., 2000.